Quantifying the impact of heat loss, stretch and preferential diffusion effects to the anchoring of bluff body stabilized premixed flames

Combustion and Flame 237 (2022) 111729

Contents lists available at ScienceDirect

Combustion and Flame

journal homepage: www.elsevier.com/locate/combustflame

Quantifying the impact of heat loss, stretch and preferential diffusion effects to the anchoring of bluff body stabilized premixed flames

F.H. Vance*, Y. Shoshin, L.P.H. de Goey, J.A. van Oijen

Mechanical Engineering, Eindhoven University of Technology, Eindhoven, the Netherlands

ARTICLE INFO

Article history:
Received 8 November 2020
Revised 29 August 2021
Accepted 1 September 2021
Available online 22 September 2021

Keywords:
Bluff body flame
Preferential diffusion
Flame stretch
Flame anchoring
Heat loss

ABSTRACT

The response of a premixed flame subjected to either flame stretch (and associated Lewis number effects) or heat loss has been well documented in the literature and has enabled a good understanding of canonical configurations such as flat burner-stabilized, counter flow and tubular flames. However, in practical burners, flames are simultaneously subjected to stretch, heat transfer with the flame holder and preferential diffusion effects. For such flames, usually the collective effect of underlying contributions is studied and individual effects are only treated in a qualitative manner. In this paper, our objective is to use flame stretch theory to separate and quantify the underlying contributions from flame stretch, preferential diffusion and heat transfer with the flame holder to the flame speed of bluff body stabilized flames. It is shown that the theory adequately predicts the flame displacement speed in comparison to the results from the numerical simulations. Using the quantification of contributions, an overall stabilization mechanism for H_2 enriched CH_4-air mixtures is discussed. The role of competing contributions from preferential diffusion and heat loss is highlighted especially near the flame base region where the flame speed is heavily impacted by all the effects. Insights are also given for low Lewis number flashback prone flames.

1. Introduction

The manner in which a flame stabilizes has been a key subject in combustion science for almost a century. For flames that are subjected to isolated effects of either flame stretch or heat loss, a large amount of studies have generated our current detailed knowledge about flame stabilization for canonical configurations. For flames influenced only by stretch effects, the impact of mixture Lewis number on flames speed has also been well known [1–4]. However, in practical burners, flames can be subjected simultaneously to heat transfer with the flame holder, recirculation vortices, flow straining, flame curvature and Lewis number effects, which can significantly change the flame anchoring process depending on the flow conditions, burner geometry and mixture properties. For this purpose, researchers usually employ a semi-practical configuration where a bluff body [5–9] or a perforated plate [10] acts as a flame holder for the stabilization of flames. How such geometries act as flame holders has attracted much attention in the recent times especially in the context of designing fuel-flexible burners for fuels with varying Lewis numbers.

In the time frame between the pioneering studies of Lewis and von Elbe [11] and recent laminar direct numerical simulations [5,7,8,12–15], a great deal of effort has been dedicated towards the understanding of the flame anchoring process. The role of conjugate heat transfer between the fluid and the solid burner has been highlighted as crucial for flame stabilization [5,16]. It has also been proposed in Ref. [5] that the flame stabilizes where necessary 'ignition' conditions are present downstream of the bluff body. In Ref. [5] this region was observed to be inside the recirculation zone in the wake of the bluff body. However, the presence of such 'ignition' conditions have not been fully presented in the literature for laminar flames in an unsteady sense and their role in situations where no vortex is present (such as those presented recently by the authors in Ref. [17]) is highly doubted. Another point is that the role of flame stretch in anchoring of such flames has been generally downplayed. Indirect stretch effects i.e. changes in local enthalpy and elemental compositions have been identified to play a strong role near flame anchoring regions for $Le \leq 1$ turbulent and laminar flames [6,7,13,18,19]. But the contribution of these changes to the flame speed have not been evaluated so far. Michaels and Ghoniem [13] studied numerically the impact of hydrogen addition into methane flames stabilized on a bluff body. They showed that for the same equivalence ratio, flames

* Corresponding author.
E-mail address: f.h.vance@tue.nl (F.H. Vance).

https://doi.org/10.1016/j.combustflame.2021.111729

with more hydrogen in the fuel stabilize at an upstream location where the strain rates are higher. They related this movement of the flame leading edge to the higher extinction stretch rates for increasing H_2 in the fuel. However, the ability of the flame to extinct at higher stretch rates for low Lewis number mixtures is due to the stronger preferential diffusion effects and does not explain directly why the flame chooses a different location to stabilize especially in relation to heat transfer with the flame holder. Another similar investigation on ultra-lean CH_4/H_2/air mixtures was conducted in Ref. [20] for explaining anomalous blow-off as presented in Ref. [21]. The upstream movement of a flame with an increase in mixture velocity for $Le < 1$ flames was shown to arise from an increase in the local stoichiometry near the flame base resulting from strong preferential diffusion effects. However, the impact of such changes on the flame speed was not separated from the rest of the effects especially in the presence of heat loss to the burner. It was also argued in Ref. [20] that heat losses became insignificant at the blow-off for their case but the authors of Ref. [20] commented that the role of heat loss could be fundamental in the stabilization and blow-off mechanisms for other situations. This further stresses the need for a method to quantify the contributions to the flame speed such that solid interpretations can be made on the nature of flame stabilization and its relation with flow and mixture properties.

Most of the previous studies have focused on the collective response of flame speed and its relation with the flame stabilization mechanism, and have treated individual contributions of flame stretch, heat loss and Lewis number effects near the flame base region in a qualitative manner. Thus, a quantitative assessment of individual contributions from flame stretch, heat loss and Lewis number effects is missing in the literature. Such a quantification of the underlying phenomena is essential for our understanding of the flame stabilization process in a detailed manner.

In the current study, we quantify the contributions from flame stretch, preferential diffusion and heat transfer with the flame holder to the flame speed. For this purpose, we study three mixtures of CH_4/H_2/air with equal adiabatic unstretched burning velocity. This should result in flames with the same stabilization angle and stabilization mechanism, and if not, then the contribution of phenomenon causing the changes will be relatively easy to distinguish. We measure CH^* chemiluminescence and perform (steady) simulations for CH_4/H_2/air mixtures at two different inlet mixture velocities, so as to understand the effect of preferential diffusion on flame shape, stand-off distance and local flame speed. We use experiments for validating major observations and then use the validated numerical model for the major part of the analysis. In order to first evaluate the flame stabilization process in the absence of preferential diffusion effects, we remove Lewis number effects from the CFD model and compare the computed flame speed with that predicted by the flame stretch theory of de Goey and Ten Thije Boonkkamp [22] resulting from contributions of flame stretch and heat transfer with the flame holder. The understanding of flame stabilization is advanced using the complete model with inclusion of preferential diffusion effects. We quantitatively evaluate the role of stretch rate, heat loss and preferential diffusion in axi-symmetric flames and use that to better understand the flame stabilization mechanism.

The key novel objectives of this study are:

- Develop a methodology for quantification of individual contributions to the flame speed from stretch, heat transfer with flame holder and preferential diffusion for multi-dimensional flames;
- An assembled understanding of the full stabilization process using the above mentioned quantification by variation of flow velocity and mixture Lewis numbers;
- Explanation of possible causes that would make low Lewis number flames to be prone to flashback.

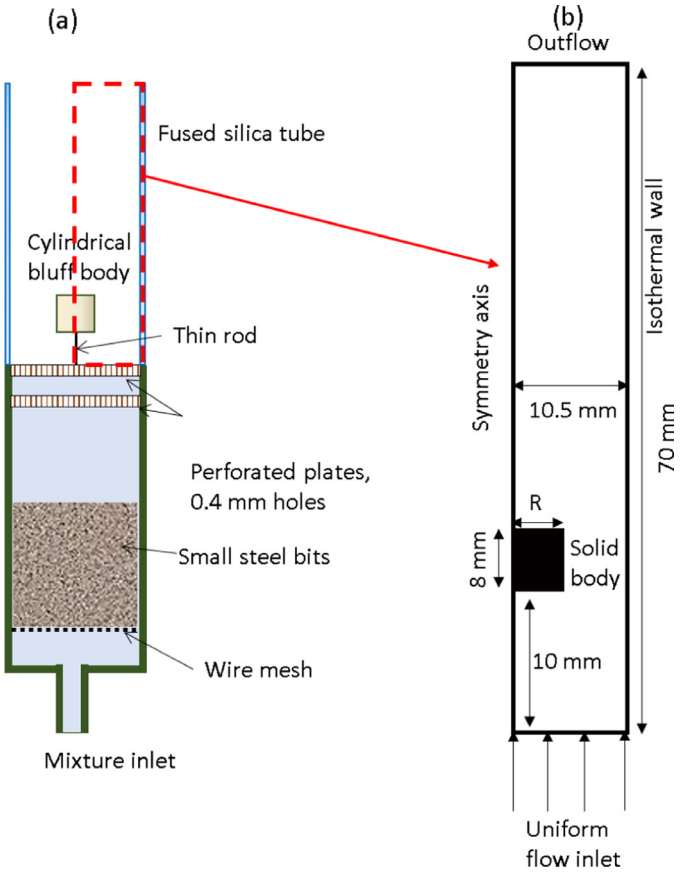

Fig. 1. Experimental setup (a) and computational model (b) with R=4 mm.

2. Experimental set-up and numerical model

Experimental setup used in this work is shown in Fig. 1(a) and is the same as used in our previous studies [7,17]. The premixed mixture passes through a cylindrical plenum chamber where initial turbulence is dissipated by a 30 mm layer of small steel beads at the bottom. A uniform flow profile is generated by two perforated plates of 21.5 mm diameter, with holes of 0.4 mm diameter installed at the plenum chamber outlet. Supported by a 0.4 mm diameter steel rod, a cylindrical bluff body made of brass with a diameter of $D = 2R = 8$ mm and a height of 8 mm acts as a flame holder. In this work, brass is chosen as the material of the flame holder to allow contributions from both stretch and heat loss effects on the flame speed. Usage of a material with low conductivity (such as ceramic flame holder) would have resulted in negligible heat losses when the steady state is reached. In order to protect the flame from external flow and from dilution of the mixture with the surrounding air, a glass tube of fused silica with 21.5 mm internal diameter is installed. To qualitatively evaluate local flame shape and burning rates, flame images were captured with a black and white camera operated in 14 bit mode. An interference filter centered at the wavelength of 430 nm near the maximum of CH^* radical chemiluminescent emission band, with a transmission band of 10 nm is used. Flame images are then Abel-inverted for comparing the relative volumetric radiation intensities with the results from numerical simulations. Accuracy of the mass flow controllers used in the experiment is 1% of the flow rate.

The numerical configuration is based on the experimental setup and the geometry is shown in Fig. 1(b). The inlet velocity is fixed

Table 1
Cases presented with $S_L = 10.4$ cms^{-1}.

α	Fuel	V_{in}[ms^{-1}]	ϕ	$T_{b,0}$[K]
0	CH_4	1	0.58	1632
0	CH_4	0.5	0.58	1632
0.2	0.2 H_2 + 0.8 CH_4	1	0.55	1594
0.2	0.2 H_2 + 0.8 CH_4	0.5	0.55	1594
0.4	0.4 H_2 + 0.6 CH_4	1	0.52	1546
0.4	0.4 H_2 + 0.6 CH_4	0.5	0.52	1546

at 0.5 m s^{-1} and 1 m s^{-1} which corresponds to an inlet Reynolds number of 259 and 518, respectively, for the case of the methane flame. The geometry is modelled as an axi-symmetric 2D slice. The solid bluff body is modelled as an axi-symmetric 2D slice as well, with the axis of rotation at the center-line of the bluff body and with boundary conditions ensuring conservation of energy at the interface between solid and fluid domains. The wall of the enclosing tube is modelled as an isothermal no-slip wall with a temperature of 300 K. This external wall in the experiments corresponds to a glass tube with a low thermal conductivity and all the flames presented in this study do not interact with this wall except for the downstream sections. These downstream sections do not change the flame structure near the flame base (which is the main focus of this study) and thus, the boundary condition of 300 K is justified. The outlet is modelled with a Neumann type boundary condition implying that there is no change in the field variables in the normal direction. Conjugate heat transfer of the fluid with the solid bluff body (thermal conductivity, $k = 109$ W/K m) is also modelled. The steady equations are solved using the SIMPLE algorithm with a finite volume solver and a second-order upwind discretisation scheme using Ansys Fluent [23]. It is to be noted that all flames presented in this study were steady and stable. This was confirmed by experiments and also by using an unsteady solver for some of the flames presented here. This was done based on the observation presented in Ref. [24] that steady solver could suppress intrinsic instabilities. Chemistry for CH_4/H_2/air flames is modelled using the DRM19 mechanism [25] which contains 21 species and 84 reactions which provides a good balance between numerical cost and accuracy. Constant Lewis number based mixture properties are used [26] based on conclusions from [27,28] that the assumption of constant Lewis number based transport properties are in good agreement when compared with the mixture-averaged properties. Constant Lewis numbers are calculated by simulating one-dimensional flat flames using mixture-averaged properties using CHEM1D [29].

The reacting flow equations are solved on an equidistant structured grid with a 100 µm global grid resolution. A two-level grid refinement is applied based on the temperature gradient resulting in a local resolution of 25 µm in the flame zone. The thermal thickness of the flames is ≈1 mm for the three mixtures considered in this study. This results in almost 40 cells in the flame thermal zone and in well resolved solutions. In this study we use experimental results for validation of numerical simulations and the subsequent detailed analysis is done using numerical results.

The percentage of H_2 in the fuel is characterised by α, given by $\alpha = \frac{X_{H_2}}{X_{H_2}+X_{CH_4}}$, where X_{H_2} and X_{CH_4} are the molar fractions of H_2 and CH_4 in the fuel, respectively. The six cases presented in this study are shown in Table 1 with varying percentage of hydrogen α, and two inlet mixture velocities V_{in}. The adiabatic burning velocity, S_L is chosen equal to $S_L = 10.4$ cms^{-1} by varying the fuel equivalence ratio for each α. This results in lower equivalence ratios for $\alpha = 0.2,\ 0.4$ cases and hence slightly lower adiabatic flame temperatures $T_{b,0}$. The flame is numerically ignited by specifying a high temperature patch near the rear end of the bluff body for the pure CH_4 flame and then using this result as an initial condition for H_2 enriched flames and lower inlet velocities.

3. Comparison of numerical results with experiments

In this section, experimentally measured CH* chemiluminescence which serves as a marker for heat release rate in a qualitative manner is compared with heat release rate from numerical simulations. Figure 2 shows the experimentally measured CH* chemiluminescence (after applying Abel inversion) and numerically obtained heat release rate for all cases. For numerical simulations, we use the full model with conjugate heat transfer between the burner and the gas as well as inclusion of preferential diffusion effects. Maximum heat release rates from the respective simulations are used to scale the local heat release rates. The difference in thickness of reaction zone in experiments and simulations is due to the difference in compared quantities (CH* versus heat release rate) and resolutions of each method. Experimental results are less resolved than the numerical simulations. It should be noted from the experimental profiles that all flames presented here are stable and symmetric around the axis. This justifies the use of a steady solver and modelling of a 2D slice for these conditions.

It can be observed from Fig. 2 that the distance of the flame from the axis of symmetry increases with increasing hydrogen content in the mixture and with decreasing inlet mixture velocities, both numerically and experimentally. The flames with hydrogen present in the fuel, burn strongly near the flame base and stabilize closer to the bluff body despite the mixture and laminar flame velocity being the same.

A detailed comparison between flame shapes from experiments and simulations is shown in Fig. 3 where dashed lines mark experimental result while solid lines mark numerical results. The flame shape is determined by the location of maximum heat release rate and maximum CH* intensity at various heights. The flame leading edge location is calculated by the intersection of the flame iso-line with the iso-contour of 10% of the maximum intensity and heat release rate for experiments and simulations, respectively. It can be observed that there is an excellent agreement between numerics and experiments for the flame shape. The flame stand-off distances are also predicted well by the simulations. To conclude, the numerical model accurately captures the trends in the flames presented in this study and the results from numerical model can be used to draw conclusions about the flame stabilization process by quantifying contributions to the flame speed.

4. Flame stabilization and stretch theory

In this section, we outline the basics of flame stretch theory and methodology used to separate the effects of heat transfer, direct and indirect stretch on the local flame speed. A premixed flame stabilizes when a kinematic balance between the local flame speed and the flow velocity is established. The local flame speed in multi-dimensional flames can be characterized by the density weighted displacement speed or mass burning rate, which is defined as $m = -\rho(\mathbf{v}\cdot\mathbf{n}) = \rho S_d$ for steady flames, where ρ is the density, $\mathbf{v}$ is the local gas velocity, $\mathbf{n}$ is the flame normal vector and S_d is the local flame displacement speed [30]. For taking into account the density variation in the flame zone, S_d is weighted with density change inside the flame front $S_D = \frac{\rho}{\rho_u} S_d$, where subscript u indicates the unburnt side of the flame and S_D is the density weighted displacement speed referred as the flame displacement speed in the rest of the paper. The flame displacement speed can then be compared with a reference value of a corresponding 1D flat flame S_L which is the same for all flames presented in this study. Understanding the variation of flame displacement speed and its underlying contributions can help in explaining the flame

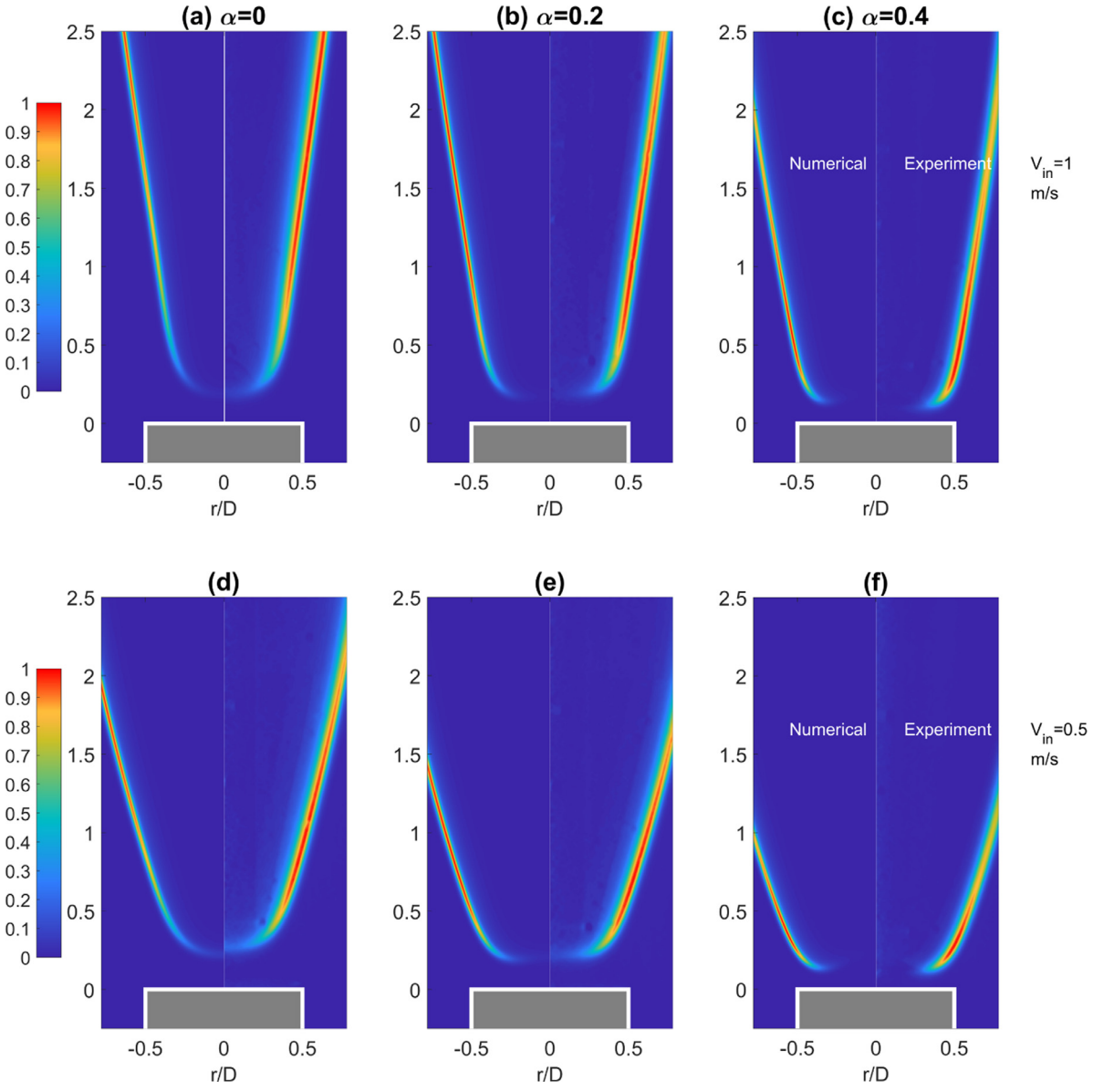

Fig. 2. Experimental CH^* chemiluminescence (right side of each subplot) and numerical scaled heat release rate (left side of each subplot) for cases $\alpha = 0,\ 0.2,\ 0.4$ at $V_{in} = 1$ ms^{-1} and $V_{in} = 0.5$ ms^{-1}, respectively, zoomed in on the flame anchoring region.

stabilization mechanism. The flame displacement speed S_D can be affected by heat loss, flow non-uniformities (i.e. strain), flame curvature and the changes in local elemental composition [22]. These changes can significantly alter the flame characteristics and stabilization mechanism. In order to characterise these changes, de Goey and Ten Thije Boonkkamp introduced a quantitative flame stretch theory [22] which takes in to account effects of stretch, heat loss and preferential diffusion on the displacement speed of the flame. Using integral analysis, they showed that the displacement speed at the burnt side of the flame front of stretched flames, $S_{D,b}$ is derived as [28]:

$$S_{D,b} = S_L(\psi_b)(1 - Ka), \tag{1}$$

where $\psi_b = (Z_{1,b}, \ldots, Z_{N_{e,b}-1}, h_b)$ represents the state at the burnt side of the flame in terms of elemental atomic composition for $j = 1, \ldots, N_e - 1$ elements in the mixture, and the enthalpy. Eq. (1) describes that the displacement speed at the burnt side $S_{D,b}$ of a stretched flame can be described by the flame speed of a stretchless flame $S_L(\psi_b)$ with enthalpy and composition on the burnt side of the stretched flame and direct stretch effects indicated by the Ka term. This relations holds for weak as well as strong stretch rates as no major assumption was made in the derivation. The displacement speed at the burnt side is used in theory because the changes in elemental composition and enthalpy inside the pre-heat zone determine the state ψ_b at which the flame will burn. Furthermore, as shown in our recent work [31], the flame displacement speed at the inner layer of the flame close to the burnt side can adequately describe the flame dynamics near the extinction limit. The Karlovitz integral Ka is a non-dimensional stretch rate and given by:

$$Ka = \frac{1}{(\sigma m^0)_b} \int_{S_u}^{S_b} \sigma Y K \rho ds, \tag{2}$$

where K is the mass based stretch rate and is linked to the local displacement speed S_d via the continuity equation as $\nabla \cdot (\rho S_d \mathbf{n}) = -\rho K$ in the flame coordinate system [30]. Karlovitz integral Ka is integrated from the unburnt to the burnt side of the flame. Y is a normalized reaction progress variable given as $Y = \frac{Y_f - Y_{f,u}}{Y_{f,b} - Y_{f,u}}$ with

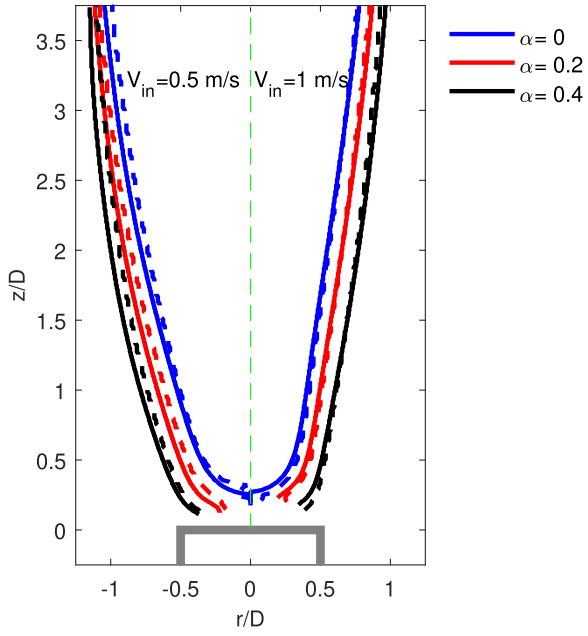

Fig. 3. Comparison between flame shape constructed using maximum heat release rate at various heights from experiments (dashed lines) and numerical simulations (solid lines).

$Y_f = Y_{CH_4} + Y_{H_2}$. κ is the curvature of the flame, related to the curvature of a small flame segment σ by $\kappa = \nabla \cdot \mathbf{n} = \frac{1}{\sigma}\frac{\partial \sigma}{\partial s}$ and $m^0 = \rho S_L$ is the mass burning rate of the respective undistorted adiabatic stretchless flame. Further, linearisation of Eq. (1) around the adiabatic undistorted state $\psi_b^0 = Z_{j,b}^0, h_b^0$ with flame speed S_L, results in an expression that is valid only for weakly stretched flames [22]:

$$\frac{S_{D,b}}{S_L} = 1 - Ka + \Delta h_b \frac{\partial}{\partial h_b^0}(\ln m_b^0) + \sum_{j=1}^{N_e} \Delta Z_{j,b} \frac{\partial}{\partial Z_{j,b}^0}(\ln m_b^0)\ (+h.o.t.). \tag{3}$$

The first two terms on the right hand side of Eq. (3) describe the direct stretch effect on the flame displacement speed. The third term describes the effect of the change in enthalpy resulting from heat loss and Lewis number effects while the fourth term describes the effect of changes in Z_j caused by preferential diffusion. Thus, Eq. (3) gives an explicit relation combining the effects of stretch rate, heat loss and preferential diffusion on the flame displacement speed. Eq. (3) can be further written as:

$$\frac{S_{D,b}}{S_L} = 1 - Ka + \sum_j \Delta\psi_j \cdot c_j\ (+h.o.t.). \tag{4}$$

The sensitivity coefficients $c_j = \frac{\partial \ln m_b^0}{\partial \psi_j}$, with $\psi = (Z_1, \ldots, Z_{N_e-1}, h)$, relate the mass burning rate of a stretchless flame m_k^0 to changes in enthalpy and elemental composition. These sensitivity coefficients can be computed by using a flamelet code (CHEM1D in this study) by varying the inlet composition and temperature of unstretched adiabatic one-dimensional flames following [1,28,32]. For this purpose, we changed the unburnt temperature T_u, equivalence ratio ϕ, mass fractions of CO_2, H_2O, CO, H_2, and O_2 in the unburnt mixture composition. These changes in the inlet parameters give different values of $\Delta\psi_{kj}$ at the inner layer of the flame. In total, 98 simulations were performed for each α (k=98) making the system of equations $\Delta\psi_{kj}c_j = \frac{m_k^0}{m^0(\psi^0)} - 1$ overdetermined with 4 unknowns and 98 equations. The overdetermined system of equations is solved using a least squares fit. Further details about the procedure for estimating sensitivity coefficients c_j can be found in previous works from our group [1,28,32]. The resulting sensitivity coefficients are presented in Table 2 for the three different values of α. The sensitivity coefficient of oxygen, c_O has a small value as compared to the hydrogen and carbon sensitivity coefficients. This results from the fuel lean conditions implying that changes in H and C, which make up the fuel composition, have more impact on the flame displacement speed.

Table 2
Sensitivity coefficients for the three different CH_4/H_2/air mixtures.

α	c_h[g]$^{-1}$]	c_C	c_H	c_O
0	4.5	180	481	-0.92
0.2	4.8	166.4	652	-1.7
0.4	5.5	177	788.4	-2.1

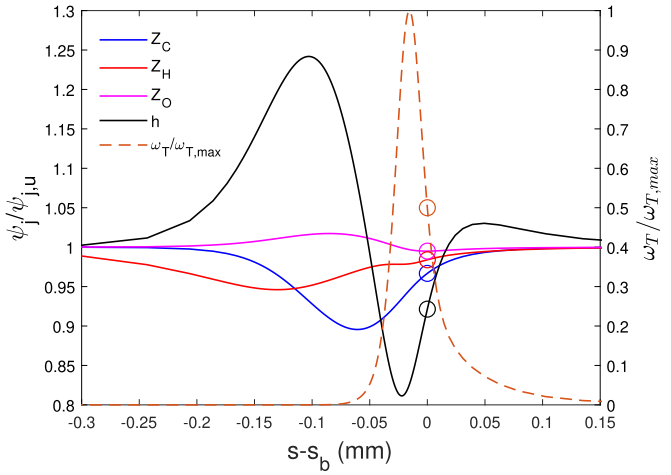

Fig. 4. Profiles of $\psi_j = (Z_C, Z_H, Z_O, h)$ along with heat release rate ω_T for a flat adiabatic unstretched flame. Reference values are marked with ◦ symbols.

In order to evaluate the changes in enthalpy and elemental mass fractions, reference values need to be computed. These reference values are taken from the undistorted adiabatic unstretched flat flame in the inner layer of the flame. This is shown in Fig. 4 for $\psi_j = (Z_C, Z_H, Z_O, h)$ scaled with unburnt values for $\alpha = 0.4$. Scaled heat release rate is also plotted as a function of flame coordinate s. For unstretched flames, $\psi_j(s \to \infty) = \psi_{j,u}$ but these values change inside the flame structure. In this study, we set the reference value as those corresponding to 50% of the maximum heat release rate on the burnt side of the flame. These values are marked with ◦ in Fig. 4 and will be used to evaluate changes in ψ_j in the 2D flame at the same value of scaled heat release rate along the flamelet path. Note that the reference values can be taken at different percentages of heat release rate or even at iso-levels of progress variable Y in the inner layer of the flame. This selection, however, will not impact the quantification of different contributions as long as the same reference location is used for 2D flames.

In the subsequent sections, we will first 'turn off' preferential diffusion in our numerical model for quantitatively evaluating the effect of the first three terms in Eq. (3) on the local displacement speed and stabilization of bluff body flames. The order for this evaluation is given below:

- Direct stretch and heat loss effects are quantified by turning off preferential diffusion effects in Section 5.
- Then the full model is used in Section 6, where direct stretch, stretch induced preferential diffusion and heat loss effects are analyzed.

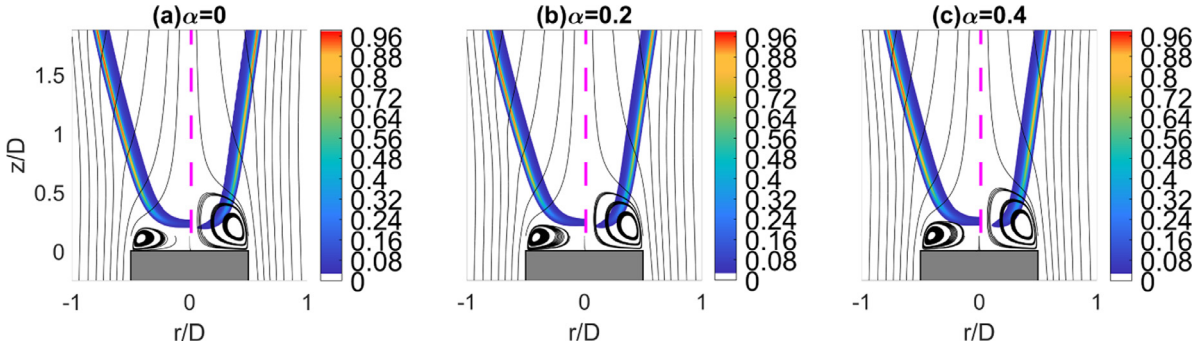

Fig. 5. Numerical scaled heat release rates with overlaid streamlines without preferential diffusion. Right half of each plot:$V_{in} = 1$ ms^{-1}. Left half of each plot: $V_{in} = 0.5$ ms^{-1}.

5. Stretch and heat loss effects without preferential diffusion

In order to build up the understanding of flame stabilization, we 'turn-off' preferential diffusion effects in the numerical model by keeping the Lewis number for all species equal to 1. Fuel equivalence ratios ϕ are updated to correct for the changes in the adiabatic burning velocity resulting from having unity Lewis number for all species. This yields $\phi = 0.585, 0.552, 0.506$ for $\alpha = 0, 0.2, 0.4$, respectively. The solution is initialized from the full model presented earlier and then solved with $Le = 1$ for all species. The displacement speed of the flame can now change due to the combined effects of stretch and enthalpy changes resulting from heat losses experienced by the flame close to the bluff body or wall. Figure 5 shows results for the scaled heat release rate with overlaid streamlines for all the cases. The maximum heat release rate is less than the adiabatic values for the cases shown, resulting from local heat losses. All flames at a given mixture velocity have the same stabilization angle. The flames shown in Fig. 5 have recirculation vortices present with similar lengths. For $V_{in} = 1$ ms^{-1}, flame base region is stabilized inside the RZ indicating that flames stabilize in an RZ stabilized regime as discussed in our recent work [17]. For $V_{in} = 0.5$ ms^{-1}, the flame region is outside the smaller RZ and thus indicates that the role of RZ in stabilization is less important here.

5.1. Heat loss and correlation with RZ

In this section, we focus on the role of the RZ in transferring heat from the flame and (hot) burnt gases to the bluff body. Near the bluff body, the flame loses heat which is transferred to the bluff body via conduction and convection through the RZ. In order to quantify this heat loss, the area integrated heat loss to the top surface of the bluff body is plotted in Fig. 6 for varying α and two inlet velocities. It is interesting to note that the heat loss is higher for higher velocity for all three mixtures. This is opposite to 1D flat burner-stabilized flames where more heat is lost at lower inlet velocity so as to reduce the displacement speed and stabilize the flame. But this behaviour is inline with our results in Ref. [17] that for RZ stabilized flames, heat loss increases with an increase in the flow velocity as heat loss is directly correlated to the recirculation zone length. Also the heat loss decreases at nearly the same rate with increase in α at a fixed inlet velocity. This slightly decreasing trend at constant velocity could be caused by the difference in T_b^0, which reduces with an increase in α and thus reduces the heat loss to the burner.

5.2. Contributions to the flame displacement speed

In this section, we focus on the direct stretch and the enthalpy heat loss of the flame and its effect on the local displacement

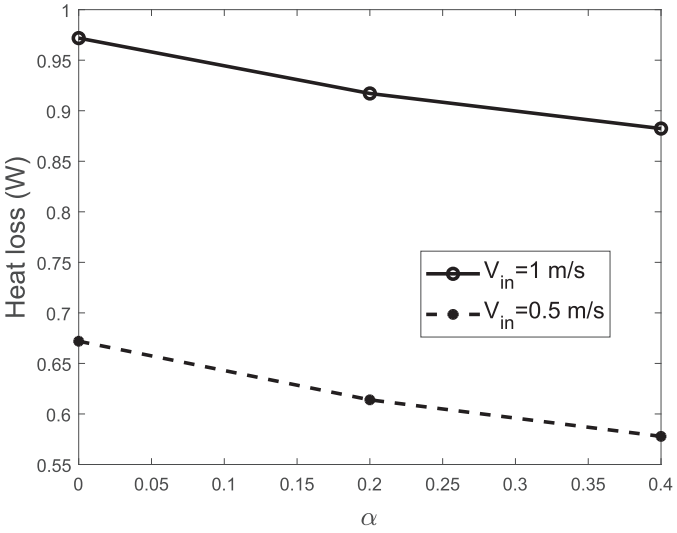

Fig. 6. Integrated heat flux to the top face of the bluff body for $Le = 1$ flames.

Table 3
Sensitivity coefficients for $\Delta Z_{j,b} = 0$.

α	c_h[Jg^{-1}]
0	3.25
0.2	3.42
0.4	3.7

speed. With $\Delta Z_{j,b} = 0$ in Eq. (3), the flame displacement speed is now dependent on both the local Karlovitz integral and the change in enthalpy resulting from heat loss. This reduces Eq. (3) to

$$\frac{S_{D,b}}{S_L} = 1 - Ka + c_h \Delta h_b \tag{5}$$

The sensitivity coefficients $c_h = \frac{\partial}{\partial h_b}(\ln m_b^0)$ are computed by increasing the unburnt temperature of adiabatic unstrained 1D flames from 300 K to 350 K, and adding CO_2 and H_2O to the unburnt mixture [1]. Since $Le_i = 1$, the values are different from the values in Table 2. The resulting sensitivity coefficients are presented in Table 3. The sensitivity coefficient, c_h, slightly increases with increasing α resulting from the difference in T_b^0.

Next we use the sensitivity coefficients and estimate $S_{D,b}/S_L$ using Eq. (5) and compare the result with results from numerical simulation. The enthalpy change $\Delta h_b = h_b - h_b^0$ is determined by calculating the enthalpy at the burnt side of the flame at the position where the heat release rate is 50% of the maximum value for both reference 1D unstretched flames (h_b^0) and 2D bluff body flames (h_b). For evaluating the Karlovitz integral Ka, the flame structure needs to be resolved and local flamelet paths have to be

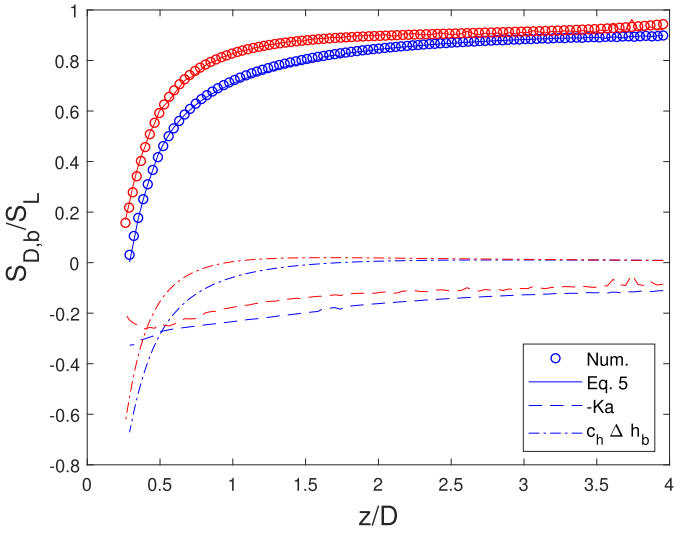

Fig. 7. Contributions from stretch and heat loss to the reduction in flame speed for $\alpha = 0$ along the flame (z/D). Results for $V_{in} = 1$ ms^{-1} and $V_{in} = 0.5$ ms^{-1} are coloured with blue and red, respectively.

constructed. Such a construction results in profiles of σ, ρK, S_D/S_L and Y. Such profiles are calculated for almost 200 flamelets along the flame length and Karlovitz integrals are evaluated for quantifying the integral effect of direct stretch in bluff body stabilized flames presented in this study.

The results are plotted in Fig. 7 as a function of axial distance downstream of the bluff body for $\alpha = 0$ for both inlet velocities (along with individual contributions from heat loss $c_h \Delta h_b^0$ and stretch rate Ka). The contribution by stretch is lower for the lower velocity case. At the flame base region between $0.25 < z/D < 1.25$, the displacement speed increases rapidly for both mixture velocities. In the region $0.25 < z/D < 0.5$, heat loss dominates the contribution to $S_{D,b}/S_L$ for both mixture velocities. The flame with $V_{in} =$ 1 m/s has a larger section of the flame which is affected by heat loss than the $V_{in} = 0.5$ m/s case. This results in more heat loss from the flame for higher velocity cases. This heat is then transferred via the RZ to the flame holder. In the region $0.5 < z/D < 1.25$, contribution from stretch in lowering displacement dominates. At the downstream section of the flame, i.e. for $1.25 < z/D < 4$, the heat loss (contribution) goes to zero and the flame speed is only affected by stretch, whose contribution is almost the same for both inlet velocities and results in $S_{D,b}$ reaching 80–90% of the adiabatic burning velocity.

It can be concluded from this section that the theoretical model is in excellent agreement with the numerical results for $S_{D,b}/S_L$ and hence can be used to understand the separate contributions of heat loss and stretch at various sections of the flame. An understanding of the role of RZ and heat loss coupled with stretch rate has been developed, which will be helpful in analysing the flames with preferential diffusion in the next section.

6. Stretch, heat loss and preferential diffusion effects

In this section, we return to the full model described in Section 4 and analyse the different contributions to the flame displacement speed arising from stretch, heat loss and preferential diffusion effects in a systematic way. We make use of the results from previous sections as a base for understanding the additional effect of preferential diffusion.

6.1. Preferential diffusion

Preferential diffusion effects arise from the difference in diffusivities of the species and can significantly change the local stoichiometry in the flame [33]. Elemental mass fractions Z_j are conserved quantities as they can neither be created nor destroyed by chemical reactions. However, under strain and curvature effects, locally the elemental mass fractions are not conserved [1,5,6] in premixed flames leading to different fractions at the burnt and unburnt side. In order to analyze the overall effect of these changes on the local stoichiometry, the local equivalence ratio ϕ_{local} scaled with inlet value is plotted in Fig. 8(a)–(c). The local equivalence ratio is defined as:

$$\phi_{local} = \left(\frac{\xi}{1-\xi}\right) \Big/ \left(\frac{\xi_{st}}{1-\xi_{st}}\right). \tag{6}$$

Here, the subscript st represents the stoichiometric conditions and ξ is the Bilger's mixture fraction defined as [34]:

$$\xi = \frac{2M_C^{-1}Z_C + 0.5M_H^{-1}Z_H - M_O^{-1}(Z_O - Z_{O,2})}{2M_C^{-1}Z_{C,1} + 0.5M_H^{-1}Z_{H,1} + M_O^{-1}Z_{O,2}}. \tag{7}$$

Here, subscripts 1 and 2 refer to fuel and oxidizer and M_j is the atomic mass of element j. In Fig. 8(a)–(c), it can be observed that the maximum value of $\phi_{local}/\phi_{in} - 1$ occurs just at the flame base region for all flames. This is the same region where major elemental changes are also present due to higher stretch rates. Another observation to make is that the maximum change in local equivalence ratio increases with an increase in α due to stronger preferential diffusion effects. For $\alpha = 0.4$, the maximum change in ϕ_{local} is about 10% near the flame base. These changes in ϕ_{local} can significantly affect the flame displacement speed and their contribution is quantified in Section 6.4.

6.2. Heat loss

With $Le = 1$ for all species, it was observed that the heat loss to the bluff body was higher for higher inlet velocity and decreased slightly with an increase in α. With $Le \neq 1$, the integrated heat loss to the top surface of the bluff body is plotted in Fig. 9 for the 6 cases listed in Table 1. The heat loss to the bluff body is again higher for higher inlet velocity. However, with an increase in α, the difference between the heat loss at two velocities becomes smaller contrary to what is observed in the previous section. These results when compared with results from Fig. 8 and response of 1D stretched flames [1] indicate that higher heat losses for higher α are caused by more intense burning near the flame base resulting from preferential diffusion effects. This strong relationship between heat loss manifested by the enthalpy changes and preferential diffusion effects will be quantified in the next section.

6.3. Stabilization mechanism

In this section, we present a summary outlining the flame stabilization mechanism as derived from the results in the previous sections. At the flame base region, due to higher stretch rates, preferential diffusion effects are stronger. With decreasing mixture Lewis number, due to an increase in preferential diffusion contribution at the same stretch rate, the flame moves upstream to find a different anchoring position. With the flame moving closer to the flame holder, more heat is lost to the top surface of the flame holder, which counters the enhancement in flame speed due to preferential diffusion. This countering is essential, as the flame will continue to move upstream if it cannot lower the flame speed by losing heat. With decreasing inlet flow velocity, as stretch decreases with a decrease in mixture velocity, the flame moves upstream to

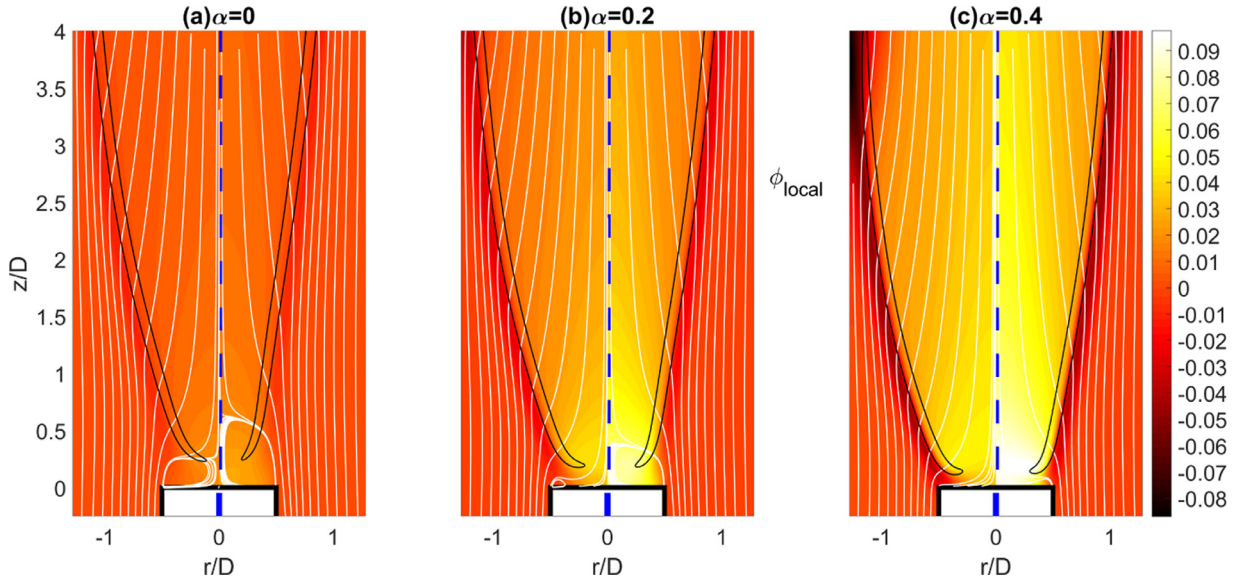

Fig. 8. Change of local equivalence ratio ϕ_{local} scaled by inlet value for three different mixtures. Left side of each sub-plot is result for lower velocity $V_{in} = 0.5$ ms^{-1} while right side is for higher velocity $V_{in} = 1$ ms^{-1}.

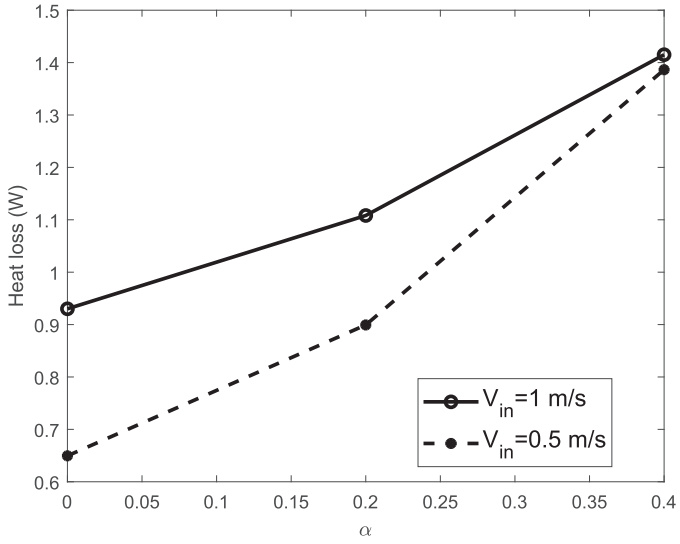

Fig. 9. Integrated heat loss to the top face of the bluff body for flames with preferential diffusion.

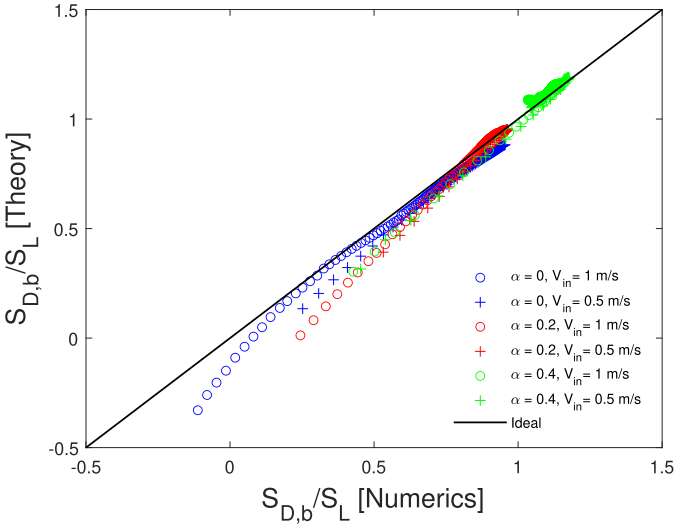

Fig. 10. Comparison between $S_{D,b}/S_L$ from numerical simulation and predicted from Eq. (3) along 200 different flamelets for the six cases presented in this study.

lower its flame speed by losing heat. An increase in heat loss to the top face of flame holder results in an increasing pre-heating effect from the side walls. This heat is transported back to the flame via the side face of the flame holder (this pre-heating increases the flame speed in regions near the flame base). The resulting balance between flame speed and local flow velocity determines if the flame will stabilize or move further upstream eventually resulting in flashback if the increase in the flame speed is not neutralized.

6.4. Quantifying contributions to the flame speed

In this section, we will quantitatively evaluate the effect of each term in Eq. (3) on the local flame displacement speed in the presence of direct stretch, heat loss and preferential diffusion effects and in turn on the stabilization of bluff body flames with different $CH_4 - H_2$-air mixtures. In Fig. 10, an overall comparison between displacement speed from numerical simulations and prediction from Eq. (3) is presented. It can be observed that there is overall good agreement between numerics and theory predictions. For $S_{D,b}/S_L > 0.5$ an excellent comparison can be observed while for $S_{D,b}/S_L \leq 0.5$ theory over-predicts the flame speed but still is in overall good agreement with the numerical simulations results.

A comparison between $S_{D,b}/S_L$ from numerical simulations and predictions by the full theoretical model is plotted in Fig. 11 as a function of the axial distance downstream of the bluff body. We again observe very good overall agreement between the theoretically predicted $S_{D,b}$ from Eq. (3) and that obtained from the numerical solutions. Some slight differences near the low $S_{D,b}/S_L$ points are observed again as in Fig. 10, specially for the cases where a recirculation zone is present. Contributions from stretch, heat loss and preferential diffusion effects to $S_{D,b}/S_L$ are also plotted in Fig. 11 (a)–(c) for $\alpha = 0, 0.2, 0.4$ flames, respectively. It can be observed that for $\alpha = 0$ at $V_{in} = 1$ ms^{-1}, near the flame leading edge, the main contribution in reducing the displacement speed is from heat loss. The stretch contribution does not change drastically throughout the length of the flame and its effect in reducing $S_{D,b}$

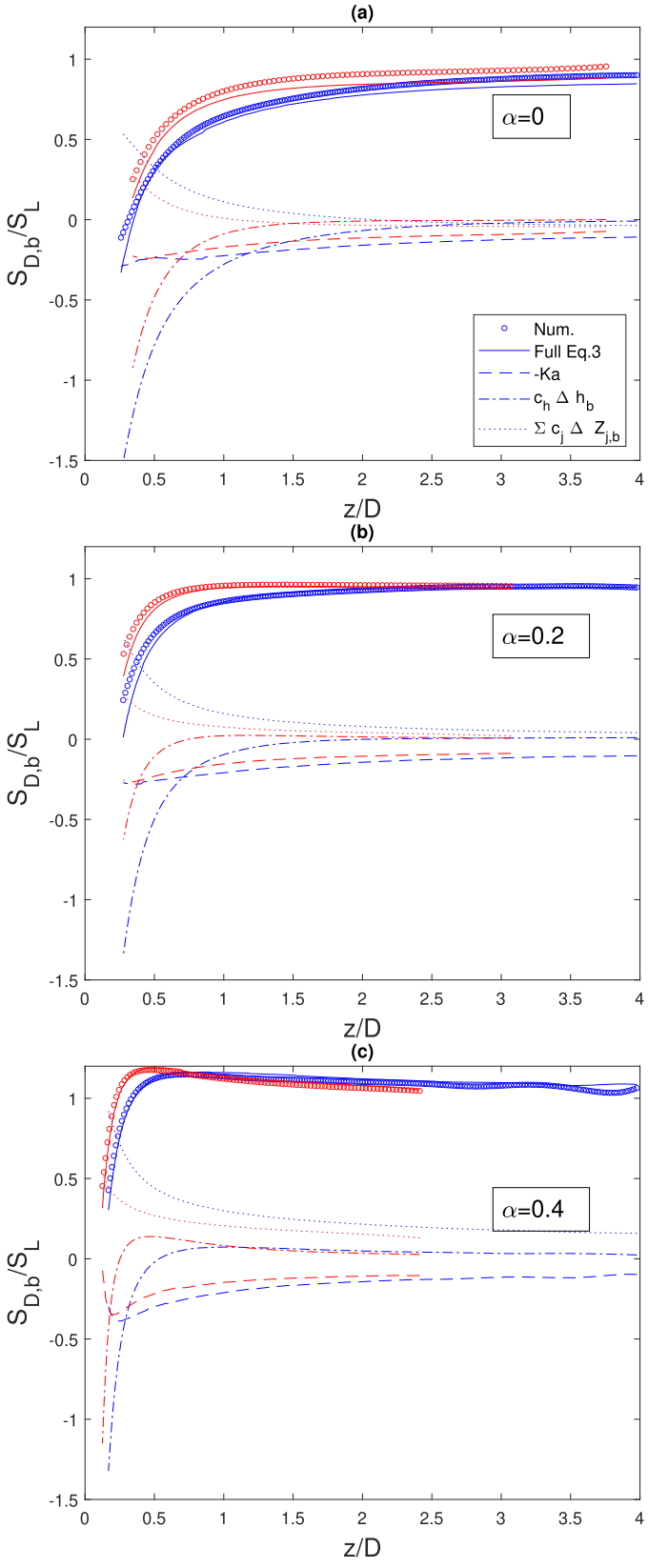

Fig. 11. Different contributions to flame displacement speed $S_{D,b}$ from Eq. (3) and numerical mass burning rate for (a) $\alpha = 0$, (b) $\alpha = 0.2$, (c) $\alpha = 0.4$. Results for $V_{in} = 1$ ms^{-1} and $V_{in} = 0.5$ ms^{-1} are coloured with blue and red, respectively.

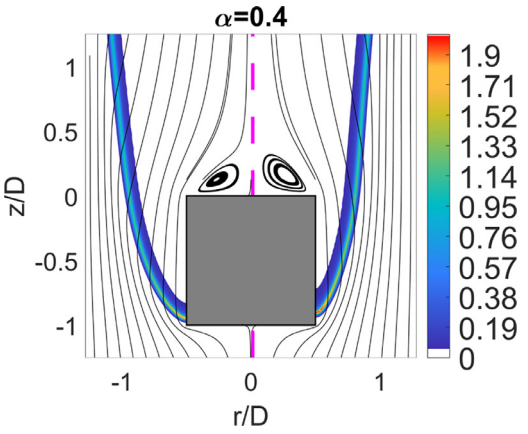

Fig. 12. Numerical scaled heat release rate with overlaid streamlines for simulations without heat loss and including preferential diffusion for $\alpha = 0.4$. Right side:$V_{in} = 1$ ms^{-1} Left side: $V_{in} = 0.5$ ms^{-1}.

is less than that of heat loss. The quantitative contribution from heat loss is higher for higher velocity as also observed in Fig. 9. This occurs simultaneously with the enhancement in $S_{D,b}/S_L$ by the preferential diffusion term, primarily due to the increase in ΔZ_C, which is higher for the higher velocity case resulting from higher stretch rates. This enhancement is countered by a larger heat loss contribution along with slightly higher stretch contribution. Just downstream of the bluff body between $0.5 < z/D < 2$, heat loss and preferential diffusion contributions decrease with increasing distance from the bluff body and further downstream, i.e. $z/D > 2$, only stretch contributes to the reduction in $S_{D,b}/S_L$.

For the $\alpha = 0.2$ flames in Fig. 11 (b), the different contributions follow a similar trend as for $\alpha = 0$ flames near the leading edge, but the overall part of the flame affected by heat loss is smaller. Subsequently, the resulting $S_{D,b}/S_L$ is higher near the flame leading edge as compared to $\alpha = 0$. For $\alpha = 0.4$, as shown in Fig. 11(c), the flames experience even much more enhancement in $S_{D,b}$ by preferential diffusion. The contribution from direct stretch is larger as compared to the other α cases. This is because the flame leading edge stabilizes at large radius near the bluff body sharp edge as seen in Fig. 2. The enthalpy term becomes similar for both velocities in agreement with Fig. 9, while the part of the flame affected by heat loss is still different. A small positive contribution by the enthalpy change for the lower velocity case near $z/D = 0.3$ and for higher velocity case at $z/D = 0.6$ can be observed. This results from intense local pre-heating coming from the side face of the bluff body due to higher heat loss. Note that pre-heating is not explicitly separated from the overall enthalpy contribution but based on the estimation of enthalpy contribution towards the flame speed for 1D stretched flames for the $\alpha = 0.4$ mixture (such as shown in Fig. 12 Ref. [28] for $\alpha = 0.4$ at $\phi = 0.6$, where the enthalpy contribution is negative for positively stretched flames), it can be argued that the increase in enthalpy contribution in Fig. 11(c) for the lower velocity case is due to pre-heating. Overall, in the flame base region, $S_{D,b}/S_L$ becomes greater than 1 for both mixture velocities. The downstream section of the flame, i.e. $z/D > 1$, is now affected both by stretch and stretch induced preferential diffusion, which is larger than the direct effect. The sum of these contributions results in $S_{D,b}/S_L \geq 1$ even near the downstream outflow boundary with direct and indirect stretch effects cancel each other.

For the flames presented in this study, it can be observed that stretch induced preferential diffusion and heat loss are the two main contributors towards the flame speed. However, the small differences in the direct stretch rates, although directly do not contribute significantly but their resulting indirect stretch effects man-

ifested mainly by the changes in elemental mass fractions are in competition with the heat loss contribution. This mechanism becomes more important as the Lewis number of the mixture is decreased.

6.5. Extreme effect of preferential diffusion in the absence of heat loss

With the increase in the contribution from preferential diffusion near the flame leading edge, it is interesting to find out how important the contribution from heat loss is in countering the enhancement from preferential diffusion. For this purpose, simulations without heat loss to the bluff body are performed by prescribing a zero heat flux boundary condition on the bluff body walls and removing conjugate heat transfer. Thus, the flame can anchor only via aerodynamic anchoring conditions. The results for $\alpha = 0$ and 0.2 are presented in Supplementary Material and briefly summarized here. For $\alpha = 0$, the flames show a slight increase in local burning near the flame base as compared to the results from Section 5. For $\alpha = 0.2$, the flames burn stronger near the flame base than the case with heat loss but the anchoring location remains on the downstream side of the bluff body. However, the $\alpha = 0.4$ flames show a very high increase in the burning rate near the flame base. The results for $\alpha = 0.4$ at both inlet velocities are shown in Fig. 12. Scaled heat release rate and streamlines are shown and it can be seen that the flame now stabilizes near the upstream edge of the bluff body where the flow speed is higher compared to the downstream edge. This is in contrast to Fig. 2, where the flame stabilizes on the top surface of the burner in the presence of heat loss effects. The scaled heat release rate is almost twice that of the maximum value of the 1D flame. As the flame is not affected by heat loss, the enhancement in S_D by stretch induced preferential diffusion is not neutralized by heat loss and the flame propagates upstream into the cylindrical volume between the bluff body and the side wall, where the flow velocity is higher due to smaller area. At the upstream corner of the bluff body, velocity gradients induce stretch effects which enhance the flame speed such that a local kinematic balance is achieved between flame speed and flow velocity. This directly shows how important the contribution from heat transfer is as we add more hydrogen into natural gas and how individual contributions to the flame speed can further help determining the effect of burner geometry (and material) on the flame stabilization process.

7. Conclusions

In this study, contributions to the flame speed from direct stretch, stretch-induced preferential diffusion and heat transfer with the flame holder have been quantified for bluff body stabilized flames with the same adiabatic burning velocities but different mixture Lewis numbers. It is shown that the flame displacement speed calculated by the theory is in good agreement with that from the numerical simulations for the current range of parameters. Using the quantified contributions to the flame speed, an overall assembled understanding of the flame stabilization process is presented. It can be concluded from this study that the flame can adjust its speed by moving to different locations near the flame holder in a complicated manner by adjusting the contributions from stretch, heat transfer with the flame holder and preferential diffusion. The quantification of contributions to the flame speed for such adjustments allows for a deeper level of understanding which can help in designing better burners for fuel-flexible combustion. This can be achieved by identifying sensitivity of individual flame speed contributors to the flame holder design parameters as the flashback or blow-off limit is reached from higher/lower velocities. However, such a design algorithm requires further research and our study can serve as the starting point for such an endeavour.

Declaration of Competing Interest

The authors declare that they have no known competing financial interests or personal relationships that could have appeared to influence the work reported in this paper.

Acknowledgments

The authors would like to express their gratitude to the Netherlands Organisation for Scientific Research (NWO) for their financial support under Project no. 13549.

Supplementary material

Supplementary material associated with this article can be found, in the online version, at doi:10.1016/j.combustflame.2021.111729.

References

[1] J.A.M. de Swart, G.R.A. Groot, J.A. van Oijen, L.P.H. de Goey, J.H.M.T.T. Boonkkamp, Detailed analysis of the mass burning rate of stretched flames including preferential diffusion effects, Combust. Flame 145 (2006) 245–258.
[2] C. Law, Combustion physics, Cambridge University Press (2006).
[3] T. Poinsot, D. Veynante, Theoretical and numerical combustion, second edition, R T Edwards, 2005.
[4] Z. Chen, Effects of hydrogen addition on the propagation of spherical methane/air flames: a computational study, Int. J. Hydrog. Energy 34 (2009) 6558–6567.
[5] K.S. Kedia, A.F. Ghoniem, The anchoring mechanism of a bluff-body stabilized laminar premixed flame, Combust. Flame 161 (2014) 2327–2339.
[6] R.S. Barlow, M.J. Dunn, M.S. Sweeney, S. Hochgreb, Effects of preferential transport in turbulent bluff-body-stabilized lean premixed CH_4/air flames, Combust. Flame 159 (2012) 2563–2575.
[7] F.H. Vance, Y. Shoshin, J.A. van Oijen, L.P.H. Goey, Effect of Lewis number on premixed laminar lean-limit flames stabilized on a bluff body, Proc. Combust. Inst. 37 (2019) 1663–1672.
[8] B.J. Lee, C.S. Yoo, H.G. Im, Dynamics of bluff-body-stabilized premixed hydrogen/air flames in a narrow channel, Combust. Flame 162 (2015) 2602–2609.
[9] J. Wan, H. Zhao, Blow-off mechanism of a holder-stabilized laminar premixed flame in a preheated mesoscale combustor, Combust. Flame 220 (2020) 358–367.
[10] K.S. Kedia, A.F. Ghoniem, Mechanisms of stabilization and blowoff of a premixed flame downstream of a heat-conducting perforated plate, Combust. Flame 159 (2012) 1055–1069.
[11] B. Lewis, G. von Elbe, Stability and structure of burner flames, J. Chem. Phys. 75 (1943).
[12] K.S. Kedia, A.F. Ghoniem, The blow-off mechanism of a bluff-body stabilized laminar premixed flame, Combust. Flame 162 (2015) 1304–1315.
[13] D. Michaels, S.J. Shanbhogue, A.F. Ghoniem, The impact of reactants composition and temperature on the flow structure in a wake stabilized laminar lean premixed CH_4/H_2/air flames; mechanism and scaling, Combust. Flame 176 (2017) 151–161.
[14] S. Chaudhuri, S. Kostka, M. W.Renfro, B. M.Cetegen, Blowoff dynamics of bluff body stabilized turbulent premixed flames, Combust. Flame 157 (2010) 790–802.
[15] M. Miguel-Brebion, D. Mejia, P. Xavier, F. Duchaine, B. Bedat, L. Selle, T. Poinsot, Joint experimental and numerical study of the influence of flame holder temperature on the stabilization of a laminar methane flame on a cylinder, Combust. Flame 172 (2016) 153–161.
[16] S. Berger, F. Duchaine, L. Gicquel, Bluff-body thermal property and initial state effects on a laminar premixed flame anchoring pattern, Flow Turbul. Combust. 100 (2018) 561–591.
[17] F.H. Vance, Y. Shoshin, J.A. van Oijen, L.P.H. Goey, Flame stabilization regimes for premixed flames anchored behind cylindrical flame holders, Proc. Combust. Inst. 38 (2021) 1983–1992.
[18] M.J. Dunn, R.S. Barlow, Effects of preferential transport and strain in bluff body stabilized lean and rich premixed CH_4/air flames, Proc. Combust. Inst. 34 (2013) 1411–1419.
[19] R.S. Barlow, M.J. Dunn, G. Magnotti, Preferential transport effects in premixed bluff-body stabilized CH_4/H_2 flames, Combust. Flame 162 (2015) 727–735.
[20] C. Jimenez, D. Michaels, A.F. Ghoniem, Stabilization of ultra-lean hydrogen enriched inverted flames behind a bluff-body and the phenomenon of anomalous blow-off, Combust. Flame 191 (2018) 86–98.

[21] Y. Shoshin, R. Bastiaans, L.P.H. de Goey, Anomalous blow-off behavior of laminar inverted flames of ultra-lean hydrogen-methane-air mixtures, Combust. Flame 160 (2013) 565–576.
[22] L.P.H. de Goey, J.H.M.T.T. Boonkkamp, A flamelet description of premixed laminar flames and the relation with flame stretch, Combust. Flame 119 (1999) 253–271.
[23] Ansys®fluent 17.2 User's guide, ANSYS Inc., Canonsburg, PA, 15317, USA.
[24] L. Berger, K. Kleinheinz, A. Attili, H. Pitsch, Characteristic patterns of thermodiffusively unstable premixed lean hydrogen flames, Proc. Combust. Inst. 37 (2019) 1879–1886.
[25] A. Kazakov, M. Frenklach, Reduced reaction sets based on GRI-Mech 1.2, University of California at Berkeley, USA. http://combustion.berkeley.edu/drm/. Accessed 18.09.2021.
[26] M. Smooke, V. Giovangigli, Reduced reaction sets based on GRI-Mech 1.2, Springer Verlag, 1991.
[27] N. Burali, S. Lapointe, B. Bobbitt, G. Blanquart, Y. Xuan, Assessment of the constant non-unity lewis number assumption in chemically-reacting flows, Combust. Theor. Model. 20 (2016) 632–657.
[28] J.A. van Oijen, A. Donini, R.J.M. Bastiaans, J.H.M.T.T. Boonkkamp, L.P.H. de Goey, State-of-the-art in premixed combustion modeling using flamelet generated manifolds, Prog. Energy Combust. Sci. 57 (2016) 30–74.
[29] CHEM1D. A one dimensional laminar flame code. Eindhoven University of Technology 2021.
[30] L.P.H. de Goey, R.M.M. Mallens, J.H.M.T.T. Boonkkamp, An evaluation of different contributions to flame stretch for stationary premixed flames, Combust. Flame 110 (1997) 54–66.
[31] F.H. Vance, Y. Shoshin, J.A. van Oijen, L.P.H. Goey, A physical relationship between consumption and displacement speed for premixed flames with finite thickness, Proc. Combust. Inst. 38 (2021) 2215–2223.
[32] J.A.M. de Swart, Modeling and analysis of flame stretch and preferential diffusion in premixed flames, Eindhoven University of Technology, 2009. PhD thesis
[33] F. Halter, C. Chauveau, I. Gökalp, Characterization of the effects of hydrogen addition in premixed methane/air flames, Int. J. Hydrog. Energy 32 (2007) 2585–2592.
[34] R.W. Bilger, S.H. Starner, R.J. Kee, On reduced mechanisms for methane-air combustion in nonpremixed flames, Combust. Flame 80 (1990) 135–149.